

# SLLN: Semantic-aware Low-light Image Enhancement Network

Mingye Ju, Charles A. Guo, Chuheng Chen, Jinshan Pan, Jinhui Tang, and Dacheng Tao

**Abstract**—How to effectively explore semantic feature is vital for low-light image enhancement (LLE). Existing methods usually utilize the semantic feature that is only drawn from the semantic map produced by high-level semantic segmentation network (SSN). However, if the semantic map is not accurately estimated, it would affect the high-level semantic feature (HSF) extraction, which accordingly interferes with LLE. In this paper, we develop a simple yet effective two-branch semantic-aware LLE network (SLLN) that neatly integrates the random intermediate embedding feature (IEF) (i.e., the information extracted from the intermediate layer of semantic segmentation network) together with the HSF into a unified framework for better LLE. Specifically, for one branch, we utilize an attention mechanism to integrate HSF into low-level feature. For the other branch, we extract IEF to guide the adjustment of low-level feature using nonlinear transformation manner. Finally, semantic-aware features obtained from two branches are fused and decoded for image enhancement. It is worth mentioning that IEF has some randomness compared to HSF despite their similarity on semantic characteristics, thus its introduction can allow network to learn more possibilities by leveraging the latent relationships between the low-level feature and semantic feature, just like the famous saying "God rolls the dice" in Physics Nobel Prize 2022. Comparisons between the proposed SLLN and other state-of-the-art techniques demonstrate the superiority of SLLN with respect to LLE quality over all the comparable alternatives.

## I. INTRODUCTION

High-quality images are crucial in a large number of computer vision applications, such as tracking [1], segmentation [2], detection [3], etc. Unfortunately, when images are captured under low-light conditions, there is typically impairment by visual distractions or catastrophic loss of information detail. To mitigate this issue, many low-light image enhancement (LLE) methods have been proposed recently.

Currently emerged LLE technologies can be roughly categorized into two groups: model-based methods and learning-based methods.

**Model-based Methods:** The most representative model used in LLE methods is Retinex model [4]. This model

assumes that an image  $I$  can be constructed by the illumination map  $U$  and reflectance map  $R$ , which can be expressed by:

$$I = R \cdot U, \quad (1)$$

where  $\cdot$  denotes element-wise multiplication. According to this model, numerous implementations have been reported [5]–[12]. For example, Guo *et al.* [6] proposed low-light image enhancement (LIME), which refined the coarse illumination map by imposing a structure prior on Retinex model. In [12], Li *et al.* used smooth prior to reconstruct LLE problem into an optimization function involving noise distribution, and thus a high-quality result can be acquired. These model-based LLE methods are capable of producing satisfactory results for some cases. However, as the hand-craft priors do not fully exploit the properties of clear images, they may induce unrealistic artifacts in the enhanced results, especially when dealing with images with inhomogeneous illumination.

**Learning-based Methods:** With the sharp development of deep learning, we have witnessed significant progress in learning-based LLE approaches [13]–[22]. Typically, Guo *et al.* [14] built a lightweight convolutional network to enhance low-light images by estimating an image-specific curve in an unsupervised way. Inspired by Retinex model, Wu *et al.* [22] unfolded the LLE task into a learnable network, which decomposed a low-light image into illumination and scene reflectance to recover high-quality scenes. These networks are able to realize remarkable performance on most low-light datasets. Nevertheless, they cannot reliably correct the lightness distribution in either bright or dark regions, i.e., unable to work well on images with inhomogeneous illumination.

Recently, a few semantic-guided learning-based efforts [23]–[25] have been devoted to solve this inhomogeneous illumination issue.

To the best of our knowledge, they are all based on the output map of semantic segmentation network (SSN) to exploring the interaction between low-level feature and semantic feature. For instance, Liang *et al.* [23] imported the enhanced image into SSN to produce a semantic map, and then combined this map and its ground truth to design a semantic brightness loss to assist the training of network. Another solution advocated by [24] is based on semantic information extracted from the output map of SSN to guide the adjustment of low-level feature. Its main advantage is that it does not require the ground truth of semantic segmentation map to participate during training, which makes it easier to implement compared to [23]. Although this kind of algorithm alleviates the limitation of inhomogeneous illumination to some extent, their results are still prone to inevitable poor

Mingye Ju is with Nanjing University of Science and Technology, Nanjing 210094, China, and also with Nanjing University of Posts and Telecommunications, Nanjing 210000, China (e-mail: jumingye@njupt.edu.cn).

Charles A. Guo is with University of New South Wales, Sydney, NSW 2052, Australia (e-mail: guocharl@gmail.com).

Chuheng Chen is with Nanjing University of Posts and Telecommunications, Nanjing 210000, China (e-mail: ch.chenchuheng@gmail.com).

Jinshan Pan and Jinhui Tang are with Nanjing University of Science and Technology, Nanjing 210094, China (e-mail: jsan@njust.edu.cn; jinhui-tang@njust.edu.cn).

Dacheng Tao is with the University of Sydney, 6 Cleveland St, Darlingtown, NSW 2008, Australia (e-mail: dacheng.tao@sydney.edu.au).

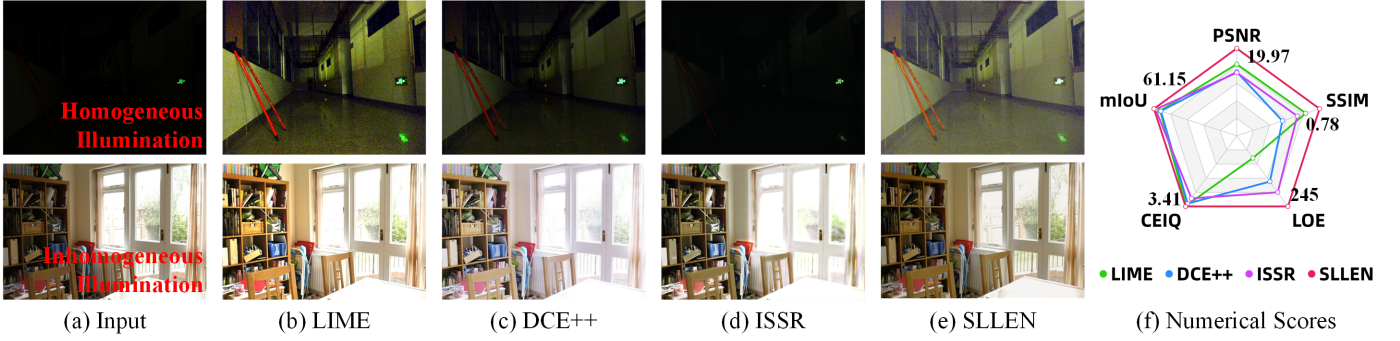


Fig. 1: The comparisons between the proposed SLLen and three most representative state-of-the-art techniques, including LIME (model-based) [6], DCE++ (learning-based) [26], and ISSR (semantic-guided learning-based) [24]. (a)~(e): Visual comparison on two given examples; As shown, the results of the proposed SLLen are superior in terms of contrast, exposure, and color, while the results of others are either under-enhanced or over-enhanced. (f): The average scores of different methods in terms of PSNR, SSIM, LOE, CEIQ, and mIoU on several commonly-used datasets remarked in Subsections III-B and III-C; it can be easily noticed that our SLLen remarkably outperforms these competitors.

visual effects. This is since SSN might lose efficacy for some cases, which may make its outputs impossible to provide the accurate semantic feature.

**Our motivation and contributions:** As aforementioned, currently available LLE algorithms usually lack the ability to effectively handle the images under inhomogeneous illumination conditions, even with the help of high-level semantic feature (HSF) fixedly extracted from the output map of SSN. Actually, random semantic information may perform better than such fixed HSF, which has been proved in previous related research, e.g., the performance of random membership degree based fuzzy C-means [27] is clearly superior to that of fixed centers based K-means. Motivated by this, a simple but effective LLE network (SLLen) is developed. It not only employs the HSF extracted from semantic segmentation map, but also utilizes random semantic information, i.e., the intermediate embedding feature (IEF) grasped from the intermediate layer in SSN, to guide network training. The main contributions of this paper are as follows:

- We propose a simple yet effective two-branch semantic-aware LLE network (SLLen) to accurately preserve the information in bright regions and light up the details in dim parts, under the guidance of both the fixed HSF and the random IEF.
- We utilize an attention mechanism to introduce HSF into low-level feature and estimate two vectors from IEF to adjust low-level feature using a non-linear manner.
- We devise a knowledge distillation loss, illumination total variation loss, and gradient loss, to constrain the SLLen for better performance.
- Extensive experiments demonstrate that the proposed SLLen achieves favorable performance against state-of-the-art methods in terms of restoration quality and enhancement accuracy, as a brief description in Figure 1.

## II. METHODOLOGY

### A. Overall Architecture

Recall that in the above, intermediate embedding feature (IEF) contains some random characteristics on semantic compared to high-level semantic feature (HSF), which makes it

able to more flexibly leverage the hidden interrelation between low-level feature and semantic feature. According to this fact, a semantic-aware image enhancement network (SLLen) is proposed to learn the mapping between low-light images and clear scenes. The baseline of our network is U-Net [28], and only three modules are consisted in this network, i.e., Feature Extraction Module, Feature Enhancement Module, and Decoder Module. The overall architecture of the SLLen is illustrated in Figure 2. As shown, both IEF and HSF are separately embedded into different branches to strengthen our network. Because the Decoder Module is the same as the general encoder-decoder framework [28], thus we only give a detailed introduction to the first two modules in the following.

### B. Feature Extraction Module

Three kinds of feature, i.e., low-level feature  $\mathbf{L}$ , HSF  $\mathbf{H}$ , and IEF  $\mathbf{B}$  are extracted in this module. For  $\mathbf{L}$ , it is extracted through the U-Net encoder, i.e.,

$$\mathbf{L} = f_{\text{encoder}}(\mathbf{I}), \quad (2)$$

where  $f_{\text{encoder}}$  denotes the operation of encoder. For  $\mathbf{H}$ , it is extracted from the output map of semantic segmentation network (SSN) [29]. Figure 3(a) gives an example of segmentation process of SSN, where  $\mathbf{S}$  is the semantic map obtained from SSN. To draw  $\mathbf{H}$  from  $\mathbf{S}$ , high-level semantic extraction block (HSEB) demonstrated in Figure 3(b) is designed, which involves three convolutional layers (each layer has 64, 128, and 512 filters of size  $3 \times 3$ ) and max pooling with ReLU activation. Formally, the process of HSEB can be illustrated by:

$$\mathbf{H} = f_{\text{HSEB}}(\mathbf{S}), \quad (3)$$

where  $f_{\text{HSEB}}$  stands for the operation of the HSEB.

For the last feature  $\mathbf{B}$ , here we remark that it is only picked from the intermediate layer of SSN. This is due to the fact that the feature drawn from the deeper layer in SSN is closer to  $\mathbf{H}$ , while the feature drawn from the shallower layer in SSN mainly contains more low-level features. In contrast, the



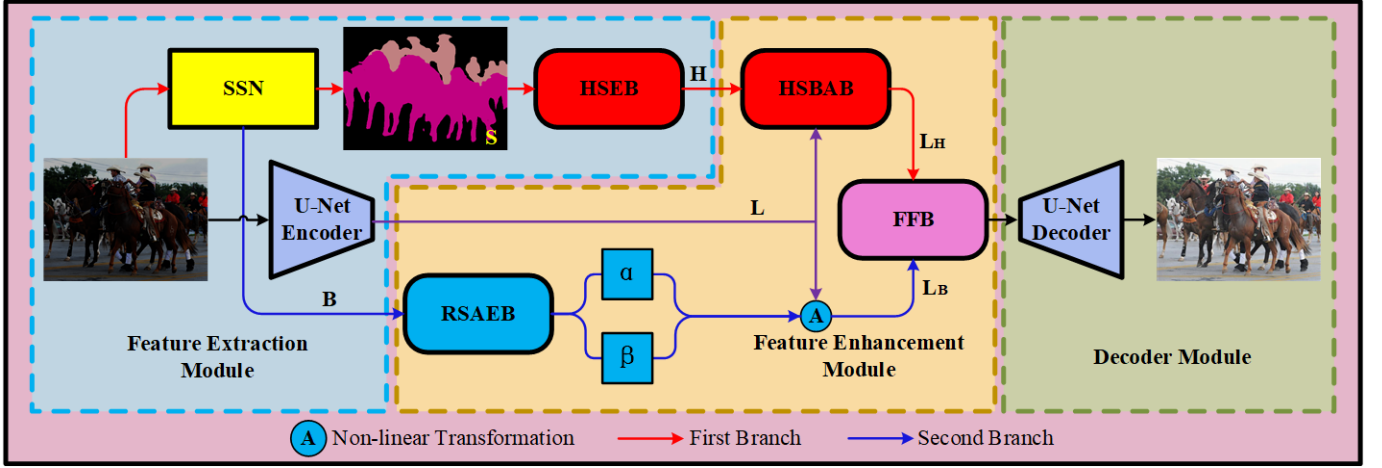


Fig. 2: An overview of our proposed SLLEN. It consists of three modules, i.e., Feature Extraction Module, Feature Enhancement Module, and Decoder Module. Two enhancement branches are included in this architecture, which are highlighted in red and blue, respectively.

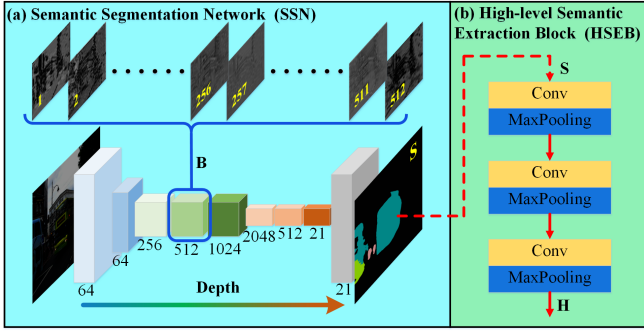


Fig. 3: The details of two blocks in Feature Extraction Module. (a): The framework of semantic segmentation network (SSN), where the  $B$  indicates the IEF grasped from the intermediate layer in SSN. (b): The framework of high-level semantic extraction block (HSEB).

intermediate embedding layer could provide some randomness under the condition of maintaining the latent semantic feature. Without loss of generality, we pulled out  $B$  with the size of  $512 \times 64 \times 64$  from the 4-th layer of SSN as the random semantic information, as demonstrated in Figure 3(a). In this case, SSN fails to produce an accurate semantic map  $S$ , leading to the errors during extracting high-level semantic feature. Unlike the  $S$ , the grasped  $B$  has 512 random semantic maps that are different from each other, which can feed more randomness to SLLEN and thus promote its generalization ability (This will be verified in Subsection III-A and the Appendix-C).

### C. Feature Enhancement Module

In this subsection, we further present a Feature Enhancement Module to enhance and fuse low-level feature and semantic feature. Figure 2 describes that this module contains three parts, including high-level semantic based attention block (HSBAB), random semantic aware enhancement block (RSAEB), and feature fusion block (FFB), where HSBAB is

in the first branch for introducing HSF into low-level feature through an attention mechanism and RSAEB is in the second branch to integrate the random IEF and low-level feature.

1) *High-level Semantic Based Attention Block*: According to the attention mechanism [30], vector  $V$  can be adjusted under the guidance of vector  $K$  using an attention map generated by mapping its vector  $Q$  to vector  $K$ . In this work, the HSBAB is introduced to implement an attention mechanism. More specifically, as illustrated in Figure 4(a),  $Q$  and  $V$  are generated from  $L$ , and  $K$  is generated from  $H$ . In this way,  $L$  can be effectively adjusted by the generated attention map, which is formulated as:

$$L_H = \text{SoftMax}\left(\frac{QK^T}{\sqrt{d_k}}\right)V, \quad (4)$$

where  $L_H$  is the optimized feature of  $L$  based on HSF  $H$ ,  $\text{SoftMax}(\cdot)$  stands for the SoftMax normalization operation, and  $d_k$  is the normalization factor. However, because of the drawback of  $H$  as discussed above, the corresponding result  $L_H$  may fail to sufficiently support the high-quality performance of LLE task (see Subsection III-A). As a result, random semantic aware enhancement block is proposed as follows.

2) *Random Semantic Aware Enhancement Block*: In [24], Fan *et al.* integrates the HSF into LLE by imposing a linear transformation on low-level feature  $L$ . Nevertheless, it unintentionally induces two complications; one is that linear transformation is not flexible enough to adjust the  $L$ , and the other is that two semantic based vectors directly calculated from the HSF have the potential to be erroneous due to the fallibility of SSN. To tackle this problem, instead of using the HSF, we adopt a non-linear transformation on low-level information with the guidance of random IEF  $B$ . Mathematically, it can be written by:

$$L_B = \beta \cdot L^\alpha, \quad (5)$$

where  $L_B$  is the adjusted feature,  $\alpha$  and  $\beta$  are non-linear transformation vectors with the size of  $1 \times 1 \times 512$  generated

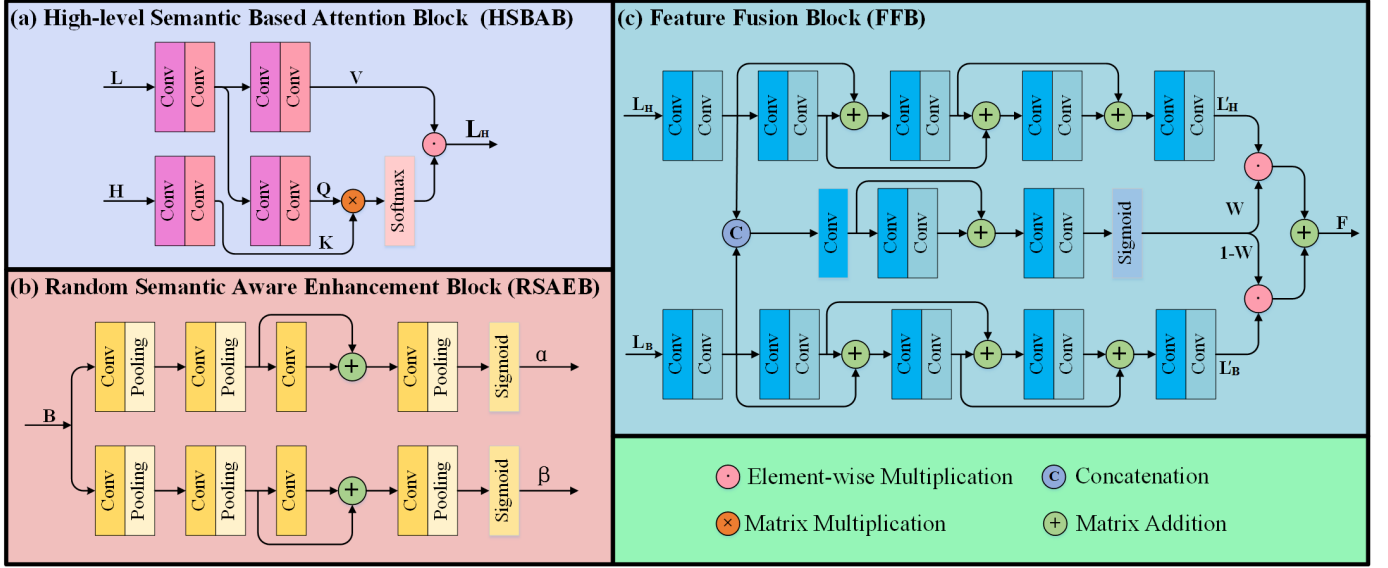


Fig. 4: The details of three blocks in the Feature Enhancement Module. (a): The framework of High-level Semantic Based Attention Block (HSBAB). (b): The framework of Random Semantic Aware Enhancement Block (RSAEB). (c): The framework of Feature Fusion Block (FFB).

from IEF **B** using several convolutional layers, as shown in Figure 4(b). Compared to the technique [24] that directly employs the HSF extracted from the output map produced by SSN, our strategy can suppress the limitations of SSN and make use of the random semantic characteristics in the IEF to better predict the two vectors, which is beneficial to leverage the inherent relationships between low-level feature and semantic feature.

3) *Feature Fusion Block*: Once  $L_H$  and  $L_B$  have been computed, we adopt a feature fusion block (FFB) to aggregate the high-level semantic aware feature  $L_H$  and semantic aware feature  $L_B$ . Figure 4(c) depicts the detailed structure of the FFB. It can be concluded from this figure that  $L_H$  and  $L_B$  can be fused through several convolution operators, and weight  $W$  is used to make a trade-off between  $L_H$  and  $L_B$ . Accordingly, this process is expressed as:

$$F = W \cdot L'_H + (1 - W) \cdot L'_B, \quad (6)$$

where  $F$  is the fused feature,  $L'_H$  and  $L'_B$  are the convolutional results in FFB. Using this strategy, the two semantic guided low-level features can be well interacted to boost the LLE generalization performance of the proposed SLEN. Finally, we reconstruct the enhanced result using fused feature  $F$  by U-Net decoder as demonstrated in Figure 2.

#### D. Loss Function

During training, the smooth loss  $\mathcal{L}_s$  [31] and the perceptual loss  $\mathcal{L}_{vgg}$  [32] are employed. Moreover, we further exploit a knowledge distillation loss  $\mathcal{L}_{kd}$ , an illumination total variation loss  $\mathcal{L}_{itv}$ , and a gradient loss  $\mathcal{L}_g$ , to improve the performance of network.

**Knowledge Distillation Loss.** According to [33], the encoder can serve as a teacher network to supervise the decoder

(student network), which makes to yield a knowledge distillation loss:

$$\mathcal{L}_{kd} = \sum_{i=1}^n \mathcal{MSE}(E_i - D_{n-i+1}), \quad (7)$$

where  $n$  is the number of layers in the encoder-decoder framework,  $E_i$  and  $D_{n-i+1}$  indicate the embedding from the  $i$ -th encoder layer and the  $n-i+1$ -th decoder layer, respectively.

**Illumination Total Variation Loss.** Based on Retinex theory [4], low-light image can be decomposed into reflectance map  $R$  and illumination map  $U$ . Here, we take enhanced image  $O$  as reflectance map  $R$ , thus  $U$  can be calculated by rewriting Eq. (1) as:

$$U = \frac{I}{O}. \quad (8)$$

In general, illumination map  $U$  tends to be smooth spatially [4]. This inspires us to propose an illumination total variation loss  $\mathcal{L}_{itv}$  to quantify the dissimilarity among the adjacent pixels in the illumination map, i.e.,

$$\mathcal{L}_{itv} = \frac{1}{CHW} \sum_{c=1}^C \sum_{h=1}^H \sum_{w=1}^W [(\nabla_x U_{c,h,w})^2 + (\nabla_y U_{c,h,w})^2], \quad (9)$$

where  $C$ ,  $H$  and  $W$  represents separately channel, height and width of  $U$ ,  $\nabla_x$  and  $\nabla_y$  are the horizontal and vertical gradient operations, respectively.

**Gradient Loss.** Following exposure control loss that proposed in [14], we design a gradient loss  $\mathcal{L}_{gra}$  to enhance the contours and textures of restored results. In detail, the loss  $\mathcal{L}_{gra}$  is defined as:

$$\mathcal{L}_{gra} = \frac{1}{3 \cdot N} \sum_{i=1}^N \|\mathbf{O}_i^g - G\|_1, \quad (10)$$

where  $\|\cdot\|_1$  indicates the  $\mathcal{L}_1$  norm,  $N$  represents the batch size,  $\mathbf{O}_i^g$  is the average gradient value of  $i$ -th image of current

batch. From this equation, it can be concluded that the goal of the gradient loss is to ensure the average gradient value of SLLen's result to be a desired level  $G$ . In this work, we set  $G = 0.051$  (please refer to the Appendix-A for why we initialize it as this value).

**Total Loss.** The total loss function of our network can be expressed as follows:

$$\mathcal{L}_{total} = \mathcal{L}_s + \mathcal{L}_{vgg} + \lambda_{kd} \cdot \mathcal{L}_{kd} + \lambda_{itv} \cdot \mathcal{L}_{itv} + \lambda_{gra} \cdot \mathcal{L}_{gra}, \quad (11)$$

where  $\lambda_{kd}$ ,  $\lambda_{itv}$ , and  $\lambda_{gra}$  are the weight parameters, which are empirically set to be 1, 5, and 1.

### III. EXPERIMENTS

**Implementation Details.** In our experiment, two public datasets (LOL-train [34] and LSRW [35]), consisting of low-light images with different exposure levels, were used to train SLLen to restore a low-quality image into a high-quality one.

We implement our framework with PyTorch on an NVIDIA 3090Ti GPU. During training, the batch size and the learning rate applied are initialized as 6 and  $1 \times 10^{-4}$ , respectively. The convolution operators used in SLLen are all set to be  $3 \times 3$ . ADAM optimizer is utilized with default parameters for the training of SLLen.

#### A. Ablation Study

To assess the effectiveness of each component of SLLen, we perform several ablation studies w.r.t. three loss functions and two enhancement branches.

**Contribution of Each Loss Function.** We conduct SLLen with various loss functions and present the corresponding results in Figure 5. As seen, the enhanced results by SLLen without  $\mathcal{L}_{kd}$  are prone to slight color cast. The absence of  $\mathcal{L}_{itv}$  tends to make the outputs suffer from visual unnaturalness. Moreover, removing  $\mathcal{L}_{gra}$  makes SLLen fail to restore the sharp contours. In contrast, the results enhanced by SLLen with all the loss functions are superior regarding color authenticity, structure preservation, and edge sharpness. Quantitative analysis of the contribution of each loss function can be found in the Appendix-C.

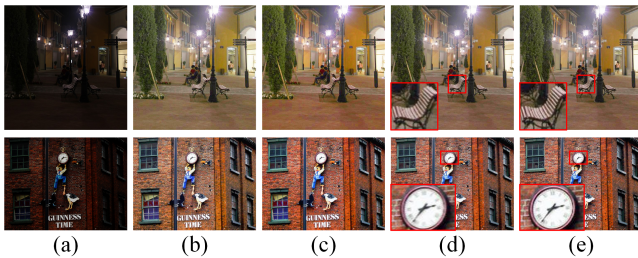


Fig. 5: Ablation study of the contribution of each loss. (a): Inputs. (b) w/o  $\mathcal{L}_{kd}$ . (c) w/o  $\mathcal{L}_{itv}$ . (d) w/o  $\mathcal{L}_{gra}$ . (e) SLLen.

**Contribution of Each Enhancement Branch.** Two feature enhancement branches are composed in the SLLen, where the first branch is to use high-level semantic feature (HSF)  $\mathbf{H}$  to guide the enhancement of low-level feature  $\mathbf{L}$  and the second branch is to impose intermediate embedding feature (IEF)  $\mathbf{B}$

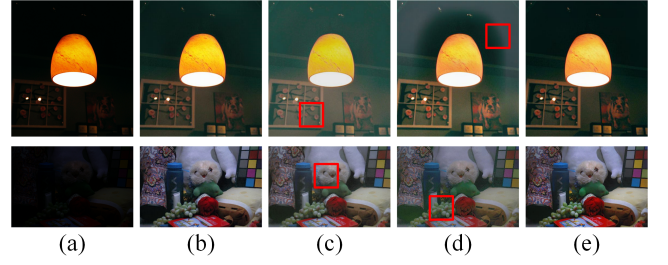


Fig. 6: Ablation study of the contribution of each branch. (a): Inputs. (b) SLLen-1 (w/o first branch). (c) SLLen-2 (w/o second branch). (d) SLLen-3 (U-Net). (e) SLLen.

on low-level feature  $\mathbf{L}$  to make SLLen more reliable. To check the efficacy of the two branches in SLLen, we implement an ablation study here. In detail, we remove the first branch (introducing  $\mathbf{H}$ ) and replace  $\mathbf{L}_H$  with  $\mathbf{L}$  as the input into the fusion block. For clarity, this ablated SLLen is marked as SLLen-1. Similarly, the second branch (introducing  $\mathbf{B}$ ) is removed and  $\mathbf{L}$  is fed into the fusion block in place of  $\mathbf{L}_B$ , and the corresponding ablated SLLen is named as SLLen-2. Finally, two branches are both eliminated, which makes SLLen degenerate into a traditional U-Net (SLLen-3). The corresponding results are shown in Figure 6.

It can be seen from the figure that SLLen-3 produces the worst results with white halos and low-contrast for the two given examples. Although SLLen-2 is able to alleviate such problems, its results are still prone to poor visibility. In comparison, SLLen and SLLen-1 win the best and second best in terms of visual quality, respectively. This corroborates that the random IEF plays a more important role than HSF in improving network's performance. Quantitative analysis of the contribution of each branch can be found in the Appendix-C.

#### B. Benchmark Evaluations

A series of experiments are conducted to investigate the performance of the proposed SLLen and other state-of-the-art methods, including LIME (model-based, TIP 2016) [6], RUAS (learning-based, CVPR 2021) [20], LTCLL (learning-based, CVPR 2021) [36], DCE++ (learning-based, TPAMI 2022) [26], UNIE (learning-based, ECCV 2022) [37], SCI (learning-based, CVPR 2022) [38], ISSR (semantic-guided learning-based, ACM-MM 2020) [24], SCL (semantic-guided learning-based, AAAI 2022) [23]. More specifically, we perform both qualitative and quantitative experiments on challenging images picked from several benchmark datasets (GladNet-Dataset (paired) [39], Synthetic Dataset (paired) [40], LOL-test (paired) [34], DICM (unpaired) [41], NPE (unpaired) [42], and MEF (unpaired) [43]).

1) **Qualitative Comparisons: Qualitative Comparison on Real-World Images.** To assess the LLE effects of SLLen, three challenging images are selected to facilitate visual and perceptual comparisons of different techniques. Both challenging low-light images and the experimental results are illustrated in Figure 7.

It is observed from Figures 7(b), (c), and (g) that LIME, RUAS, and SCI easily lead to over-restoration especially in the





Fig. 7: Qualitative comparison between the proposed SLLEN and state-of-the-art LLE techniques on three real-world examples. (a): Real-world images. (b): LIME. (c): RUAS. (d): LTCLL. (e): DCE++. (f): UNIE. (g): SCI. (h): ISSR. (i): SCL. (j): SLLEN. More comparisons can be found in the Appendix-D.

TABLE I: Quantitative comparison between SLLEN and state-of-the-art methods. (Data in bold means the best and data in red indicates the second-best.)

Metrics	Database	LIME [6]	RUAS [20]	LTCLL [36]	DCE++ [26]	UNIE [37]	SCI [38]	ISSR [24]	SCL [23]	SLLEN
PSNR $\uparrow$ / SSIM $\uparrow$	GladNet	16.9 / 0.68	14.2 / 0.59	16.1 / 0.67	15.7 / 0.48	14.5 / 0.55	<b>17.2</b> / <b>0.68</b>	15.9 / 0.63	16.2 / 0.68	<b>18.6</b> / <b>0.76</b>
	Synthetic	15.1 / 0.61	13.5 / 0.51	<b>19.5</b> / <b>0.80</b>	13.1 / 0.37	12.1 / 0.48	15.8 / 0.62	15.0 / 0.61	12.3 / 0.53	<b>18.1</b> / <b>0.79</b>
	LOL-test	17.1 / 0.67	11.3 / 0.41	17.3 / 0.66	15.0 / 0.45	<b>21.4</b> / <b>0.75</b>	13.8 / 0.53	12.4 / 0.47	13.3 / 0.61	<b>23.2</b> / <b>0.80</b>
Average PSNR $\uparrow$ / Average SSIM $\uparrow$		16.4 / 0.66	13.0 / 0.51	<b>17.6</b> / <b>0.71</b>	14.6 / 0.44	16.0 / 0.60	15.6 / 0.61	14.4 / 0.57	13.9 / 0.64	<b>20.0</b> / <b>0.78</b>
LOE $\downarrow$ / CEIQ $\uparrow$	DICM	832 / <b>3.30</b>	958 / 2.73	505 / 3.02	502 / 3.13	<b>277</b> / 3.26	362 / 3.01	521 / 3.00	392 / 3.10	<b>271</b> / <b>3.31</b>
	NPE	852 / <b>3.44</b>	842 / 3.10	394 / 3.11	571 / 3.37	<b>309</b> / 3.27	346 / 3.34	421 / 3.27	393 / 3.33	<b>264</b> / <b>3.50</b>
	MEF	603 / <b>3.37</b>	330 / 2.90	210 / 3.19	459 / 3.31	264 / 3.32	<b>202</b> / 3.18	246 / 2.78	296 / 3.14	<b>200</b> / <b>3.41</b>
Average LOE $\downarrow$ / Average CEIQ $\uparrow$		762 / <b>3.37</b>	710 / 2.91	370 / 3.11	511 / 3.27	<b>283</b> / 3.28	304 / 3.18	396 / 3.02	360 / 3.19	<b>245</b> / <b>3.41</b>

bright regions (see the first and second examples). Figures 7(d) and (e) show that LTCLL and DCE++ tend to induce low contrast in their results (see the second example). As seen in Figures 7(f), (h), and (i), although UNIE, ISSR, and SCL are able to light up the most regions, the rest part of the enhanced results still remains dim (see the third example). By comparison, as seen in Figure 7(j), SLLEN can work well on low-light images with inhomogeneous illumination and restore richer textures. (Best viewed by zooming in.)

**Qualitative Comparison on Synthesis Images.** We further evaluate the restoration quality of the proposed SLLEN and the state-of-the-art approaches on three reference datasets, i.e., GladNet-Dataset [39], Synthetic Dataset [40], and LOL-test [34]. Three low-light examples are picked to facilitate the comparison. The corresponding results are illustrated in

Figure 8.

In general, the results in Figure 8 are similar to those for real-world images illustrated in Figure 7. Most of the competitors lack the ability to enhance the dim part for the example with non-uniform illumination. On the contrary, it can highlight that the results in Figure 8(j) enhanced by SLLEN are more natural and satisfactory aesthetically with reference to the ground truth images (GT).

2) *Quantitative Comparison:* To overcome the bias caused by subjective assessment, we implement quantitative comparison using two benchmark reference metrics (peak signal-to-noise ratio (PSNR) and structural similarity (SSIM) [44]), and two non-reference metrics (lightness order error (LOE) and contrast enhancement based contrast-changed image quality (CEIQ) [45]). Table I lists the average scores of PSNR





Fig. 8: Qualitative comparison between the proposed SLLen and state-of-the-art LLE techniques on three synthesis image examples. (a): Synthesis images. (b): LIME. (c): RUAS. (d): LTCLL. (e): DCE++. (f): UNIE. (g): SCI. (h): ISSR. (i): SCL. (j): SLLen. (k): GT. More comparisons can be found in the Appendix-D.

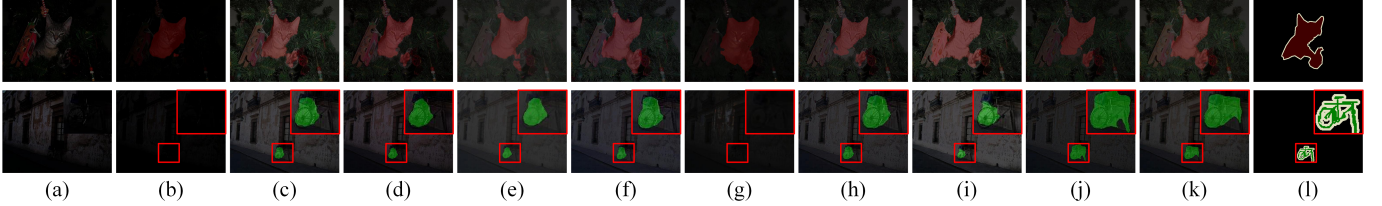


Fig. 9: Two examples of semantic segmentation results on the low-light images and enhanced outputs by different algorithms. (a): Low-light images. (b): Results of (a). (c): LIME. (d): RUAS. (e): LTCLL. (f): DCE++. (g): UNIE. (h): SCI. (i): ISSR. (j): SCL. (k): SLLen. (l): GT. More comparisons can be found in the Appendix-E.

and SSIM on three paired datasets (GladNet-Dataset [39], Synthetic Dataset [40], and LOL-test [34]), and the average scores of LOE and CEIQ on three unpaired datasets (DICM [41], NPE [42], and MEF [43]).

It can be found from this table that SLLen achieves the best average scores in terms of SSIM and PSNR, which indicates that the results of SLLen are more similar to the GT compared to those of other state-of-the-arts. Moreover, the advantages of SLLen on LOE and CEIQ further demonstrate its superiority regarding illumination correction and contrast restoration.

### C. Semantic Segmentation in the Dark

In this subsection, we evaluate the performance of state-of-the-art LLE techniques on the high-level semantic segmentation task under low-light conditions. In specific, we randomly select 100 images from visual object classes (VOC) [46] and darken them according to [36]. These darkened images are then enhanced by the aforementioned comparable methods and our SLLen. Finally, we adopt [47] as a baseline to rank the

segmentation capability for different algorithms. Figure 9 gives the semantic results on two given examples. As expected, the semantic maps of output results of SLLen are the closest to the GT compared to those of its competitors. To further facilitate the comparison, mean Intersection over Union (mIoU), whose larger value means better semantic segmentation result, is used to evaluate the performance of different algorithms on semantic segmentation. The corresponding average mIoU scores on the 100 examples by each algorithm are listed in Table II. As seen, the score of SLLen outperforms those of the eight comparable approaches.

## IV. CONCLUSION

In this work, we develop a two-branch network (SLLen) to implement low-light image enhancement (LLE), under the guidance of high-level semantic feature (HSF) and intermediate embedding feature (IEF). Among them, HSF is directly extracted from the output map of semantic segmentation network (SSN) and IEF is grasped from the intermediate

TABLE II: The average mIoU scores of semantic segmentation results on the 100 corresponding outputs enhanced by different algorithms. More specific information can be found in the Appendix-E.

Metrics	Database	LIME [6]	RUAS [20]	LTCLL [36]	DCE++ [26]	UNIE [37]	SCI [38]	ISSR [24]	SCL [23]	SLEN
mIoU $\uparrow$	100 darkened images in VOC	56.62	57.15	51.82	56.05	52.19	59.59	59.94	59.16	61.15

layer of SSN. In specific, for the first branch, an attention mechanism is utilized to integrate HSF into low-level feature. For the second branch, we estimate two vectors from IEF to drive the adjustment of low-level feature. The two adjusted features from two branches are fused together to be decoded for the final enhanced result. Unlike the other comparable works, our SLEN makes efficient use of random semantic information in IEF, making low-level feature and semantic feature well interacted. Extensive experiments demonstrate that the proposed SLEN is superior to the state-of-the-art alternatives on real-world scenes and various synthetic datasets.

#### REFERENCES

- [1] L. Liu, W. Ouyang, X. Wang, P. Fieguth, J. Chen, X. Liu, and M. Pietikäinen, "Deep learning for generic object detection: A survey," *International journal of computer vision*, vol. 128, no. 2, pp. 261–318, 2020.
- [2] R. Liu, Q. Chen, Y. Yao, X. Fan, and Z. Luo, "Location-aware and regularization-adaptive correlation filters for robust visual tracking," *IEEE Transactions on Neural Networks and Learning Systems*, vol. 32, no. 6, pp. 2430–2442, 2020.
- [3] C. Yu, J. Wang, C. Gao, G. Yu, C. Shen, and N. Sang, "Context prior for scene segmentation," in *Proceedings of the IEEE/CVF conference on computer vision and pattern recognition*, 2020, pp. 12416–12425.
- [4] E. H. Land, "The retinex theory of color vision," *Scientific American*, vol. 237, no. 6, pp. 108–129, 1977. [Online]. Available: <http://www.jstor.org/stable/24953876>
- [5] X. Fu, D. Zeng, Y. Huang, X.-P. Zhang, and X. Ding, "A weighted variational model for simultaneous reflectance and illumination estimation," in *Proceedings of the IEEE conference on computer vision and pattern recognition*, 2016, pp. 2782–2790.
- [6] X. Guo, Y. Li, and H. Ling, "Lime: Low-light image enhancement via illumination map estimation," *IEEE Transactions on image processing*, vol. 26, no. 2, pp. 982–993, 2016.
- [7] Y.-F. Wang, H.-M. Liu, and Z.-W. Fu, "Low-light image enhancement via the absorption light scattering model," *IEEE Transactions on Image Processing*, vol. 28, no. 11, pp. 5679–5690, 2019.
- [8] M. Li, J. Liu, W. Yang, X. Sun, and Z. Guo, "Structure-revealing low-light image enhancement via robust retinex model," *IEEE Transactions on Image Processing*, vol. 27, no. 6, pp. 2828–2841, 2018.
- [9] M. Ju, C. Ding, W. Ren, Y. Yang, D. Zhang, and Y. J. Guo, "Ide: Image dehazing and exposure using an enhanced atmospheric scattering model," *IEEE Transactions on Image Processing*, vol. 30, pp. 2180–2192, 2021.
- [10] M. K. Ng and W. Wang, "A total variation model for retinex," *SIAM Journal on Imaging Sciences*, vol. 4, no. 1, pp. 345–365, 2011.
- [11] X. Ren, W. Yang, W.-H. Cheng, and J. Liu, "Lr3m: Robust low-light enhancement via low-rank regularized retinex model," *IEEE Transactions on Image Processing*, vol. 29, pp. 5862–5876, 2020.
- [12] L. Xu, Q. Yan, Y. Xia, and J. Jia, "Structure extraction from texture via relative total variation," *ACM transactions on graphics (TOG)*, vol. 31, no. 6, pp. 1–10, 2012.
- [13] W. Ren, S. Liu, L. Ma, Q. Xu, X. Xu, X. Cao, J. Du, and M.-H. Yang, "Low-light image enhancement via a deep hybrid network," *IEEE Transactions on Image Processing*, vol. 28, no. 9, pp. 4364–4375, 2019.
- [14] C. Guo, C. Li, J. Guo, C. C. Loy, J. Hou, S. Kwong, and R. Cong, "Zero-reference deep curve estimation for low-light image enhancement," in *Proceedings of the IEEE/CVF Conference on Computer Vision and Pattern Recognition*, 2020, pp. 1780–1789.
- [15] Y. Jiang, X. Gong, D. Liu, Y. Cheng, C. Fang, X. Shen, J. Yang, P. Zhou, and Z. Wang, "Enlightengan: Deep light enhancement without paired supervision," *IEEE Transactions on Image Processing*, vol. 30, pp. 2340–2349, 2021.
- [16] Y. Zhang, X. Guo, J. Ma, W. Liu, and J. Zhang, "Beyond brightening low-light images," *International Journal of Computer Vision*, vol. 129, no. 4, pp. 1013–1037, 2021.
- [17] R. Wang, Q. Zhang, C.-W. Fu, X. Shen, W.-S. Zheng, and J. Jia, "Underexposed photo enhancement using deep illumination estimation," in *Proceedings of the IEEE/CVF Conference on Computer Vision and Pattern Recognition*, 2019, pp. 6849–6857.
- [18] W. Yang, S. Wang, Y. Fang, Y. Wang, and J. Liu, "From fidelity to perceptual quality: A semi-supervised approach for low-light image enhancement," in *Proceedings of the IEEE/CVF conference on computer vision and pattern recognition*, 2020, pp. 3063–3072.
- [19] C. Zheng, D. Shi, and W. Shi, "Adaptive unfolding total variation network for low-light image enhancement," in *Proceedings of the IEEE/CVF International Conference on Computer Vision*, 2021, pp. 4439–4448.
- [20] R. Liu, L. Ma, J. Zhang, X. Fan, and Z. Luo, "Retinex-inspired unrolling with cooperative prior architecture search for low-light image enhancement," in *Proceedings of the IEEE/CVF Conference on Computer Vision and Pattern Recognition*, 2021, pp. 10561–10570.
- [21] X. Xu, R. Wang, C.-W. Fu, and J. Jia, "Snr-aware low-light image enhancement," in *Proceedings of the IEEE/CVF Conference on Computer Vision and Pattern Recognition*, 2022, pp. 17714–17724.
- [22] W. Wu, J. Weng, P. Zhang, X. Wang, W. Yang, and J. Jiang, "Uretinex-net: Retinex-based deep unfolding network for low-light image enhancement," in *Proceedings of the IEEE/CVF Conference on Computer Vision and Pattern Recognition*, 2022, pp. 5901–5910.
- [23] D. Liang, L. Li, M. Wei, S. Yang, L. Zhang, W. Yang, Y. Du, and H. Zhou, "Semantically contrastive learning for low-light image enhancement," in *Proceedings of the AAAI Conference on Artificial Intelligence*, vol. 36, no. 2, 2022, pp. 1555–1563.
- [24] M. Fan, W. Wang, W. Yang, and J. Liu, "Integrating semantic segmentation and retinex model for low-light image enhancement," in *Proceedings of the 28th ACM international conference on multimedia*, 2020, pp. 2317–2325.
- [25] D. Wang, L. Ma, R. Liu, and X. Fan, "Semantic-aware texture-structure feature collaboration for underwater image enhancement," in *2022 International Conference on Robotics and Automation (ICRA)*, 2022, pp. 4592–4598.
- [26] C. Li, C. Guo, and C. C. Loy, "Learning to enhance low-light image via zero-reference deep curve estimation," *IEEE Transactions on Pattern Analysis and Machine Intelligence*, vol. 44, no. 8, pp. 4225–4238, 2022.
- [27] J. C. Dunn, "A fuzzy relative of the isodata process and its use in detecting compact well-separated clusters," 1973.
- [28] O. Ronneberger, P. Fischer, and T. Brox, "U-net: Convolutional networks for biomedical image segmentation," *International Conference on Medical Image Computing and Computer-Assisted Intervention*, 2015.
- [29] Long, Jonathan, Shelhamer, Evan, Darrell, and Trevor, "Fully convolutional networks for semantic segmentation," *IEEE TPAMI*, 2017.
- [30] A. Vaswani, N. Shazeer, N. Parmar, J. Uszkoreit, L. Jones, A. N. Gomez, L. u. Kaiser, and I. Polosukhin, "Attention is all you need," in *Advances in Neural Information Processing Systems*, I. Guyon, U. V. Luxburg, S. Bengio, H. Wallach, R. Fergus, S. Vishwanathan, and R. Garnett, Eds., vol. 30. Curran Associates, Inc., 2017. [Online]. Available: <https://proceedings.neurips.cc/paper/2017/file/3f5ee243547dee91fbd053c1c4a845aa-Paper.pdf>
- [31] A. Wald, "Statistical decision functions." 1950.
- [32] K. Simonyan and A. Zisserman, "Very deep convolutional networks for large-scale image recognition," *arXiv preprint arXiv:1409.1556*, 2014.
- [33] G. Hinton, O. Vinyals, J. Dean *et al.*, "Distilling the knowledge in a neural network," *arXiv preprint arXiv:1503.02531*, vol. 2, no. 7, 2015.
- [34] C. Wei, W. Wang, W. Yang, and J. Liu, "Deep retinex decomposition for low-light enhancement," in *British Machine Vision Conference*, 2018.
- [35] J. Hai, Z. Xuan, R. Yang, Y. Hao, F. Zou, F. Lin, and S. Han, "R2rnet: Low-light image enhancement via real-low to real-normal network," *CoRR*, vol. abs/2106.14501, 2021. [Online]. Available: <https://arxiv.org/abs/2106.14501>
- [36] F. Zhang, Y. Li, S. You, and Y. Fu, "Learning temporal consistency for low light video enhancement from single images," in *Proceedings of*

the IEEE/CVF Conference on Computer Vision and Pattern Recognition (CVPR), June 2021, pp. 4967–4976.

- [37] Y. Jin, W. Yang, and R. T. Tan, “Unsupervised night image enhancement: When layer decomposition meets light-effects suppression,” in *Computer Vision – ECCV 2022*, S. Avidan, G. Brostow, M. Cissé, G. M. Farinella, and T. Hassner, Eds. Cham: Springer Nature Switzerland, 2022, pp. 404–421.
- [38] L. Ma, T. Ma, R. Liu, X. Fan, and Z. Luo, “Toward fast, flexible, and robust low-light image enhancement,” in *Proceedings of the IEEE/CVF Conference on Computer Vision and Pattern Recognition (CVPR)*, June 2022, pp. 5637–5646.
- [39] W. Wang, C. Wei, W. Yang, and J. Liu, “Gladnet: Low-light enhancement network with global awareness,” in *2018 13th IEEE international conference on automatic face & gesture recognition (FG 2018)*. IEEE, 2018, pp. 751–755.
- [40] Y. L. Feifan Lv and F. Lu, “Attention-guided low-light image enhancement,” *arXiv preprint arXiv:1908.00682*, 2019.
- [41] C. Lee, C. Lee, and C.-S. Kim, “Contrast enhancement based on layered difference representation of 2d histograms,” *IEEE transactions on image processing*, vol. 22, no. 12, pp. 5372–5384, 2013.
- [42] S. Wang, J. Zheng, H.-M. Hu, and B. Li, “Naturalness preserved enhancement algorithm for non-uniform illumination images,” *IEEE transactions on image processing*, vol. 22, no. 9, pp. 3538–3548, 2013.
- [43] K. Ma, K. Zeng, and Z. Wang, “Perceptual quality assessment for multi-exposure image fusion,” *IEEE Transactions on Image Processing*, vol. 24, no. 11, pp. 3345–3356, 2015.
- [44] Z. Wang, A. Bovik, H. Sheikh, and E. Simoncelli, “Image quality assessment: from error visibility to structural similarity,” *IEEE Transactions on Image Processing*, vol. 13, no. 4, pp. 600–612, 2004.
- [45] J. Yan, J. Li, and X. Fu, “No-reference quality assessment of contrast-distorted images using contrast enhancement,” *arXiv preprint arXiv:1904.08879*, 2019.
- [46] M. Everingham, L. Van Gool, C. K. I. Williams, J. Winn, and A. Zisserman, “The pascal visual object classes (voc) challenge,” *International Journal of Computer Vision*, vol. 88, no. 2, pp. 303–338, Jun. 2010.
- [47] L.-C. Chen, Y. Zhu, G. Papandreou, F. Schroff, and H. Adam, “Encoder-decoder with atrous separable convolution for semantic image segmentation,” in *Proceedings of the European conference on computer vision (ECCV)*, 2018, pp. 801–818.

## APPENDIX

### A. Statistical Results on Expected Gradient Level $G$

In our work, we design a gradient loss  $\mathcal{L}_{gra}$  to desire the average gradient value of SLLen’s result to be an expected level  $G$ . To find out such  $G$ , we calculate the average gradient values of 6000 normal illumination images in datasets [34], [39], [40]. The corresponding statistical histogram is illustrated in Figure 10. It can be easily found from this figure that the average gradient value among all the selected images is 0.051, which makes us initialize  $G = 0.051$  in this work.

### B. Comparing Decomposed Illumination Maps

During training, we propose a loss function  $\mathcal{L}_{itv}$  to ensure that illumination map  $\mathbf{U}$  is as smooth as possible. To prove the effectiveness of  $\mathcal{L}_{itv}$ , we calculate the decomposed  $\mathbf{U}$  using the enhanced results  $\mathbf{O}$  of different approaches via Retinex model, i.e.,  $\mathbf{U} = \mathbf{I}/\mathbf{O}$ , where  $\mathbf{I}$  is low-light image. Meanwhile, we also compare their low-light image enhancement (LLE) performance. The experimental results on three kinds of examples (i.e., inhomogeneous illumination, homogeneous illumination, and normal illumination) are shown in Figure 11. As seen, the proposed SLLen can not only keep an excellent smoothness property, but also avoid over-exposure for clear images.

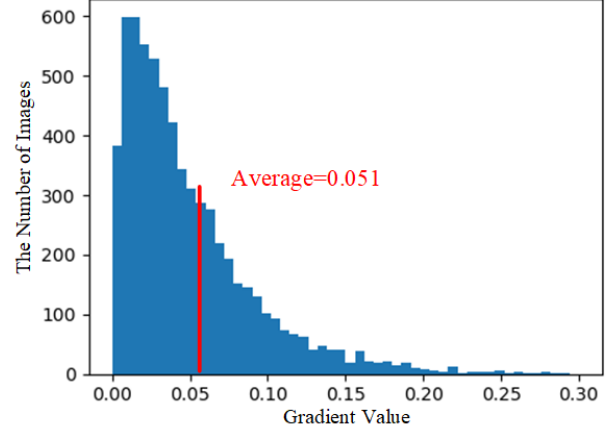


Fig. 10: The statistical histogram of 6000 normal illumination images in the datasets [34], [39], [40], where the average gradient value among all the selected images is 0.051.

TABLE III: Quantitative ablation study of the contribution of each loss, i.e., knowledge distillation loss  $\mathcal{L}_{kd}$ , illumination total variation loss  $\mathcal{L}_{itv}$ , and gradient loss  $\mathcal{L}_{gra}$ . Data in bold means the best and data in red indicates the second-best.

Metric	w/o $\mathcal{L}_{kd}$	w/o $\mathcal{L}_{itv}$	w/o $\mathcal{L}_{gra}$	SLLen
PSNR $\uparrow$	21.9	<b>22.6</b>	22.1	<b>23.2</b>
SSIM $\uparrow$	0.74	0.71	<b>0.76</b>	<b>0.80</b>
LOE $\downarrow$	<b>287</b>	288	309	<b>262</b>
CEIQ $\uparrow$	2.91	<b>2.92</b>	2.80	<b>3.14</b>

### C. Additional Ablation Study

To further investigate the effect of each component of SLLen w.r.t. three loss functions and two enhancement branches, here we use four commonly-used image quality metrics (i.e., peak signal-to-noise ratio (PSNR), structural similarity (SSIM) [44], lightness order error (LOE), and contrast enhancement based contrast-changed image quality (CEIQ) [45]), to execute several quantitative ablation studies on the dataset LOL-test [34].

**Contribution of Each Loss Function.** The comparing scores of SLLen with various loss functions are illustrated in Table III. As shown in the table, SLLen with all loss functions gives the best score, which means that the absence of each loss function leads to the deterioration of SLLen’s performance. It is also verified that the loss of the  $\mathcal{L}_{kd}$  would cause the decline of PSNR score, demonstrating  $\mathcal{L}_{kd}$  is crucial

TABLE IV: Quantitative ablation study of the contribution of each enhancement branch. Data in bold means the best and data in red indicates the second-best.

Metric	SLLen-1	SLLen-2	SLLen-3	SLLen
PSNR $\uparrow$	<b>22.2</b>	20.6	20.0	<b>23.2</b>
SSIM $\uparrow$	<b>0.75</b>	0.70	0.64	<b>0.80</b>
LOE $\downarrow$	<b>285</b>	327	433	<b>262</b>
CEIQ $\uparrow$	<b>3.13</b>	2.92	2.80	<b>3.14</b>



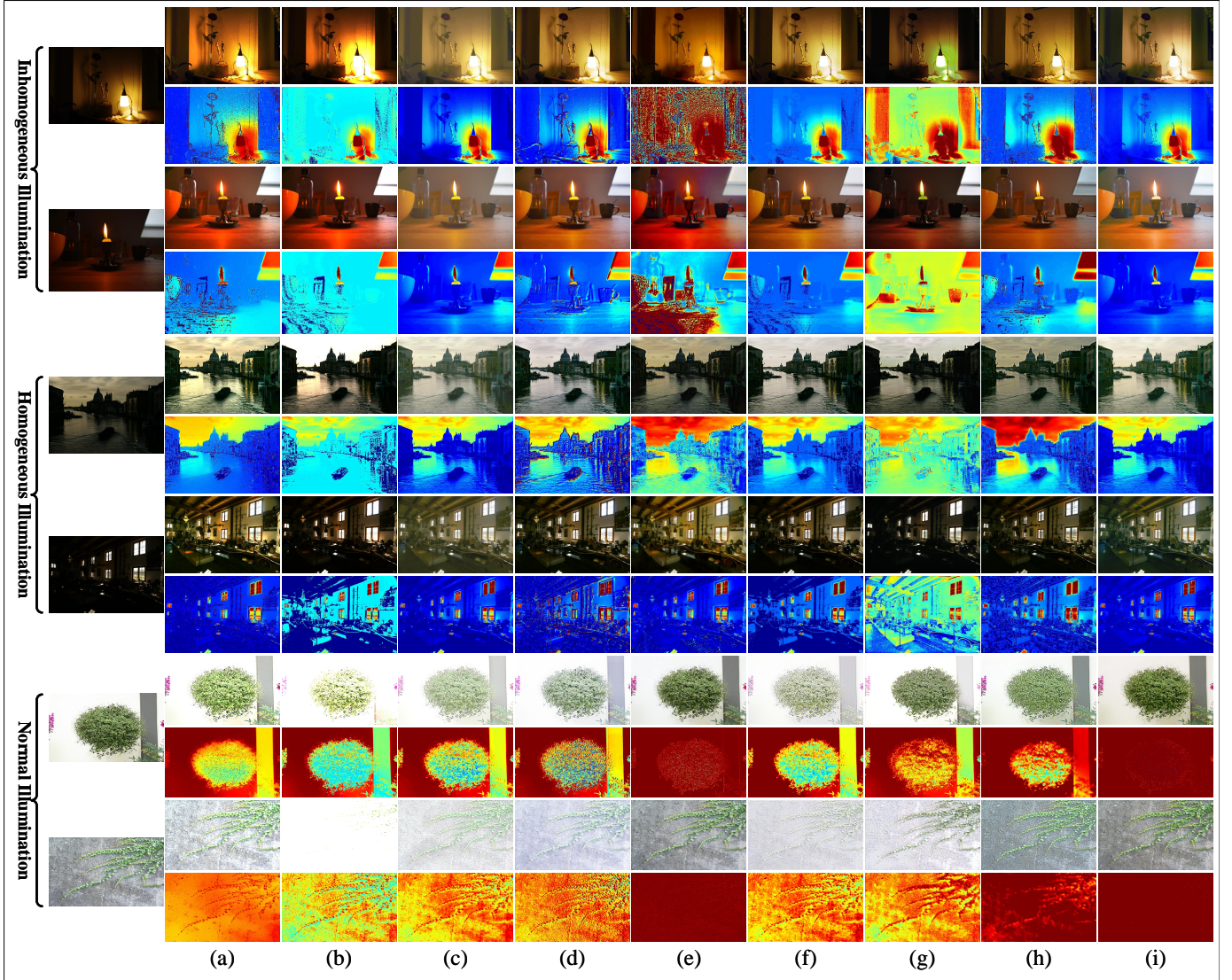


Fig. 11: The comparison on the decomposed illumination maps between the proposed SLLen and state-of-the-art LLE techniques. (a): LIME. (b): RUAS. (c): LTCLL. (d): DCE++. (e): UNIE. (f): SCI. (g): ISSR. (h): SCL. (i): SLLen.

to reviving the naturalness of enhanced images. The absence of the  $\mathcal{L}_{itv}$  brings about the decline of SSIM score, meaning that  $\mathcal{L}_{itv}$  plays an important role in structure preservation. The loss of the  $\mathcal{L}_{gra}$  mainly induces the poor scores in terms of LOE and CEIQ, which demonstrates the ability of  $\mathcal{L}_{gra}$  to restore the contrast of low-light images.

**Contribution of Each Branch.** Table IV lists the scores of SLLen-1 (w/o first branch that introduces high-level semantic feature **H**), SLLen-2 (w/o the second branch that introduces intermediate embedding feature **B**), SLLen-3 (U-Net), and SLLen. It can be checked from the table that the performance of SLLen is superior to others in terms of all the metrics, demonstrating that both enhancement branches are indispensable. It is worth mentioning that the absence of **H** only affects the LLE performance of SLLen slightly, while removing **B** is bound to seriously deteriorate the LLE ability of SLLen. This indicates **B** is dominant to the LLE performance of SLLen compared to **H**.

#### D. Additional Benchmark Evaluations

We exhibit more qualitative evaluations and a user study on the proposed SLLen and different state-of-the-art approaches, i.e., LIME (model-based, TIP 2016) [6], RUAS (learning-based, CVPR 2021) [20], LTCLL (learning-based, CVPR 2021) [36], DCE++ (learning-based, TPAMI 2022) [26], UNIE (learning-based, ECCV 2022) [37], SCI (learning-based, CVPR 2022) [38], ISSR (semantic-guided learning-based, ACM-MM 2020) [24], SCL (semantic-guided learning-based, AAAI 2022) [23].

*1) Qualitative Comparison on Real-world Images:* First of all, five real-world images are selected to conduct a qualitative comparison. The results are shown in Figure 12. It is observed from Figure 12(b) that LIME can enhance a low-quality image into a high-quality one, while this approach easily leads to over-restoration, especially in the illumination regions (see the third example). As seen in Figure 12(c), RUAS has the capability to enhance the visibility of the input images.



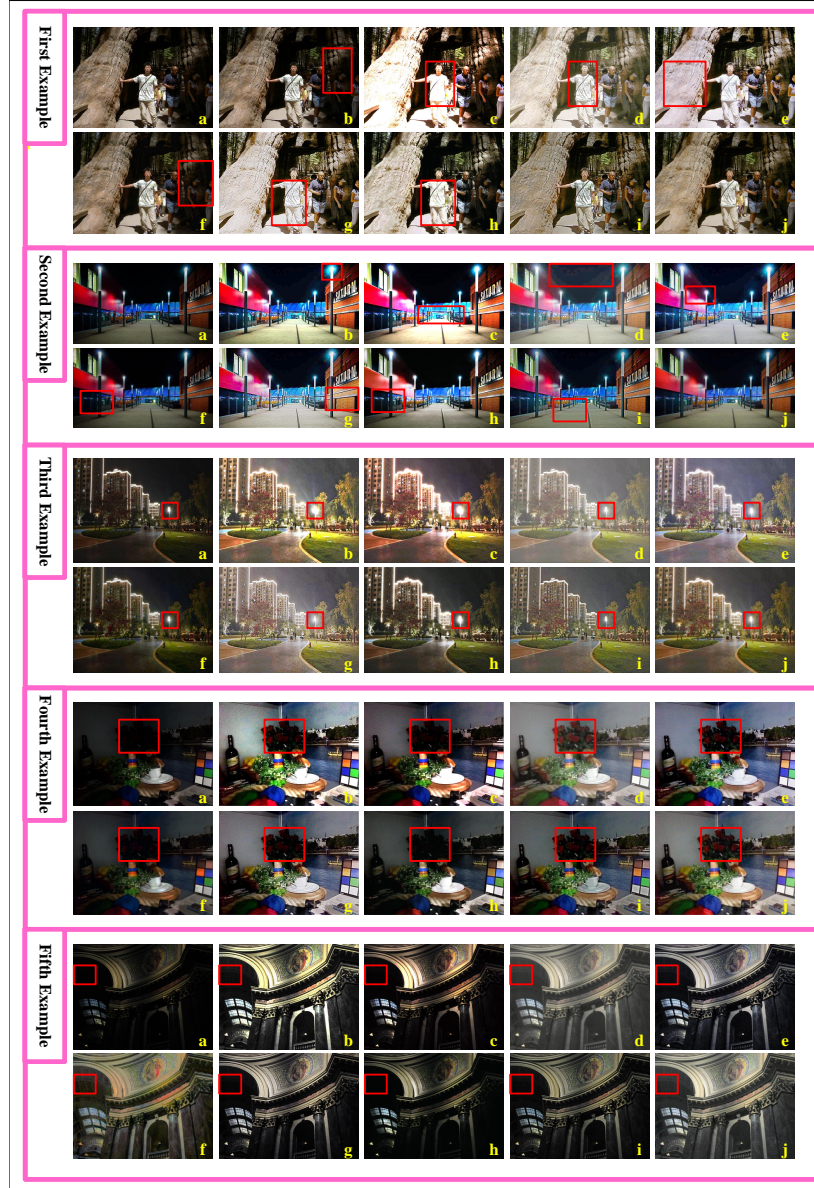


Fig. 12: Further qualitative comparison between the proposed SLEN and state-of-the-art LLE techniques on five real-world images. (a): Real-world images. (b): LIME. (c): RUAS. (d): LTCLL. (e): DCE++. (f): UNIE. (g): SCI. (h): ISSR. (i): SCL. (j): SLEN.

However, the bright regions in the results are prone to over-enhancement while the rest part of the images remains dim (see the first example). Figure 12(d) shows that although LTCLL can somewhat light up the images, it tends to induce low-contrast in the images (see the second and the fourth examples). It is observed from Figure 12(e) that DCE++ produces the pleasing enhanced images with realistic light distribution. Unfortunately, blurred details are unintentionally amplified and the dark regions remain dim (see the fifth example). In Figure 12(f), although UNIE can reconstruct the illumination distribution of the images, its results are prone to over-saturation and serious color cast (see the fifth example). As shown in Figure 12(g), SCI generates satisfactory visual results in terms of both brightness and naturalness, while it fails to effectively revive the information for dark regions,

which makes its results suffer from poor visibility (see the fourth example). As shown in Figure 12(h), ISSR effectively corrects image brightness and revives the visual details, but over-enhancement is introduced into the outputs (see the third example). For SCL shown in Figure 12(i), it enhances dark areas and attains satisfactory color of the input image, whereas it cannot light up some parts of the given examples, especially for inhomogeneous illumination images (see the fourth and the fifth examples). In contrast, as seen in Figure 12(j), SLEN can well handle images with inhomogeneous illumination and simultaneously restore the realism of regions with richer textures. (Best viewed by zooming in.)

2) *Qualitative Comparison on Synthetic Images:* In sequence, more qualitative comparison on five synthetic images is also executed on SLEN and the state-of-the-art approaches.

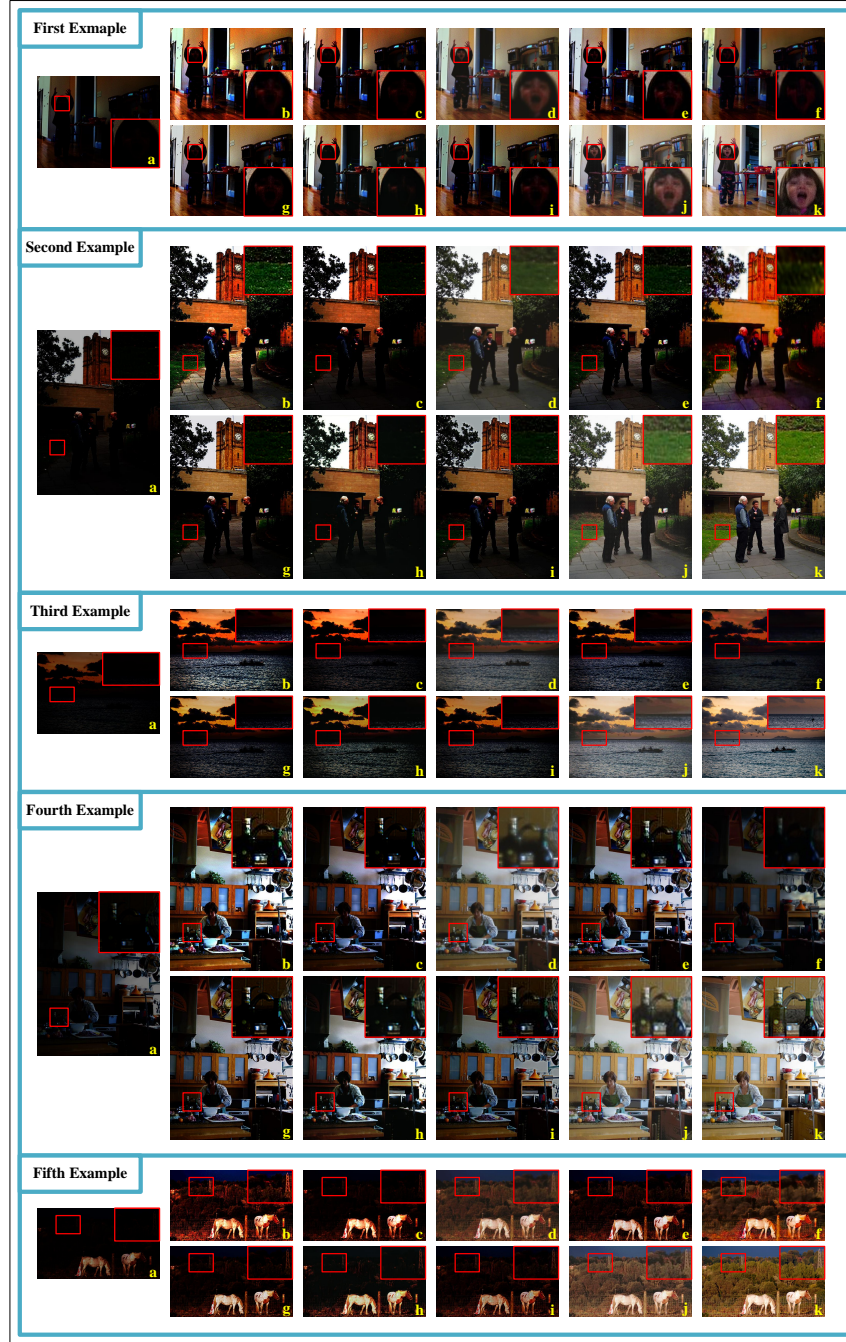


Fig. 13: Further qualitative comparison between the proposed SLEN and state-of-the-art LLE techniques on five synthetic images. (a): Synthetic images. (b): LIME. (c): RUAS. (d): LTCLL. (e): DCE++. (f): UNIE. (g): SCI. (h): ISSR. (i): SCL. (j): SLEN. (k): GT.

Figure 13 gives the qualitative comparison results. As demonstrated in Figure 13(b), the results of LIME tend to be over-saturated (see the second and the third examples). It can be drawn from Figure 13(c) that the corresponding results of RUAS still remain dark after enhancement (see the first and the fourth examples). As shown in Figures 13(d) and (e), LTCLL and DCE++ fail to enhance images with inhomogeneous illumination (see the first and the fourth examples). For UNIE shown in Figure 13(f), the corresponding results tend to be over-saturated (see the second and the fifth examples). As

shown in Figures 13(g), (h), and (i), the results produced by SCI, ISSR, and SCL are still too dim (see the first and the fourth examples). By contrast, it can highlight that the results in Figure 13(j) obtained by ours are more natural and satisfactory aesthetically with reference to the ground truth images (GT).

3) *User Study*: We also perform a user study to assess the subjective LLE ability of various techniques. We process various low-light images from the datasets (DICM [41], NPE

TABLE V: The score of the user study (US)<sup>†</sup> on the datasets (DICM [41], NPE [42], MEF [43], LIME [6], and VV) processed by different methods. Data in bold means the best and data in red indicates the second-best.

Database	LIME [6]	RUAS [20]	LTCLL [36]	DCE++ [26]	UNIE [37]	SCI [38]	ISSR [24]	SCL [23]	SLEN
DICM [41]	<b>3.852</b>	2.954	3.352	3.336	3.141	2.215	2.514	3.594	<b>4.012</b>
NPE [42]	3.213	3.057	2.923	<b>3.675</b>	3.422	3.152	2.921	3.372	<b>3.813</b>
MEF [43]	3.515	3.231	2.902	<b>3.863</b>	3.122	3.153	2.814	3.621	<b>3.932</b>
LIME [6]	3.124	2.893	3.251	<b>3.513</b>	2.546	2.823	2.587	3.245	<b>3.836</b>
VV	3.391	2.912	2.942	<b>3.924</b>	2.342	2.725	2.341	3.146	<b>4.071</b>
Average	3.419	3.009	3.074	<b>3.662</b>	2.914	2.814	2.635	3.395	<b>3.933</b>

TABLE VI: The average mIoU<sup>†</sup> scores of semantic segmentation results on the specific detected objects over 100 corresponding outputs enhanced by different algorithms on the dataset Visual Object Classes (VOC) [46]. Data in bold means the best and data in red indicates the second-best.

Detected Objects	LIME [6]	RUAS [20]	LTCLL [36]	DCE++ [26]	UNIE [37]	SCI [38]	ISSR [24]	SCL [23]	SLEN
Background	85.93	86.38	86.33	86.19	85.21	86.61	87.16	87.04	87.01
Aeroplane	71.52	59.26	49.41	55.08	49.67	65.12	55.03	72.19	64.81
Bicycle	52.07	37.38	46.93	45.88	23.76	51.54	48.70	47.73	42.94
Bird	92.64	92.94	93.94	81.47	92.22	93.22	92.13	92.96	92.77
Boat	28.50	34.77	11.10	24.55	39.71	39.16	46.15	43.42	35.90
Bottle	49.79	45.52	43.20	44.22	51.01	47.60	51.42	47.33	51.89
Bus	79.85	78.74	80.85	82.13	73.97	81.57	77.94	80.67	85.09
Car	81.29	85.51	62.63	80.14	67.45	85.93	82.61	84.65	84.56
Cat	84.20	83.83	56.80	78.23	85.55	85.38	82.74	84.91	85.59
Chair	8.28	7.30	5.83	6.55	6.70	7.84	10.12	8.61	9.35
Cow	73.91	79.52	78.08	74.37	76.37	79.75	81.52	77.92	86.54
Diningtable	55.98	56.89	74.35	71.76	53.80	59.57	64.21	59.90	68.33
Dog	49.77	49.78	34.29	54.82	37.91	58.99	53.17	59.44	65.76
Horse	53.50	58.27	59.35	57.92	55.11	56.24	54.90	57.94	60.18
Motorbike	76.90	71.50	76.42	79.12	56.27	81.02	79.40	73.45	78.69
Person	69.80	67.85	61.03	69.49	66.93	70.61	69.93	70.57	70.74
Pottedplant	23.76	11.86	10.97	19.62	7.31	17.77	18.75	22.16	21.48
Sheep	63.11	86.80	87.12	78.01	85.58	87.17	85.65	87.36	86.94
Sofa	20.43	30.87	14.42	21.34	23.90	24.73	35.68	16.46	24.96
Tvmonitor	11.09	17.98	3.28	10.10	5.31	11.98	21.58	8.42	19.46
Average	56.62	57.15	51.82	56.05	52.19	59.59	<b>59.94</b>	59.16	<b>61.15</b>

[42], MEF [43], LIME [6], and VV<sup>1</sup>) by different methods. For each low-light image, we display it on a screen and provide the outputs from the different competitors. We invite 10 human subjects to score the perceptual quality of the enhanced images. The subjects are required to consider: 1) whether the results are over-/under-exposed; 2) whether the results are pleasing aesthetically; 3) whether the results produce color deviation. The scores of perceptual quality range from 1 to 5 (worst to best quality). As summarized in Table V, SLEN wins the best average US score on the given datasets.

#### E. Additional Semantic Segmentation in the Dark

Three more experimental results from the 100 darkened images are illustrated in Figure 14. As seen, SLEN produces the best results that are the closest to the GT. Meanwhile, a detailed version of the quantitative comparisons of mean Intersection over Union (mIoU) is shown in Table VI. Here, we give the semantic segmentation results of different state-of-the-art algorithms on the specific detected objects. It can be observed in the table, the proposed SLEN, with the highest mIoU score, outperforms other approaches.

TABLE VII: Running time comparison (in second) of the proposed SLEN and different state-of-the-art methods.

Method	Running time	Platform
LIME [6]	0.05002	MATLAB (CPU)
RUAS [20]	0.00218	Pytorch (GPU)
LTCLL [36]	0.00221	Pytorch (GPU)
DCE++ [26]	0.00057	Pytorch (GPU)
UNIE [37]	0.00462	Pytorch (GPU)
SCI [38]	0.00034	Pytorch (GPU)
ISSR [24]	5.90612	TensorFlow (GPU)
SCL [23]	0.00047	Pytorch (GPU)
SLEN	0.01711	Pytorch (GPU)

#### F. Limitation and Broader Impacts

Table VII lists the running time of the different techniques averaged on 32 images of size  $512 \times 512 \times 3$ , which is measured on a PC with an Nvidia RTX 3080Ti GPU and Intel I9 12900KF CPU. As expected, due to the introduction of a semantic segmentation network [29], the proposed SLEN does not show an advantage in computational efficiency compared to some networks. However, the LLE quality and semantic extraction performance of SLEN are undoubtedly the best (see Figures 11, 12, 13, 14 and Tables V, VI). Therefore, our SLEN can serve as an excellent candidate that provides both high-quality LLE and semantic extraction services.

<sup>1</sup><https://sites.google.com/site/vonikakis/datasets>





Fig. 14: Further examples of semantic segmentation results on the low-light images and the outputs enhanced by different algorithms. (a): Low-light images. (b): Results of (a). (c): LIME. (d): RUAS. (e): LTCLL. (f): DCE++. (g): UNIE. (h): SCI. (i): ISSR. (j): SCL. (k): SLEN. (l): GT.

More importantly, to the best of our knowledge, we are the first to introduce the intermediate embedding feature containing random semantic maps that are different from each other, i.e., the information extracted from the intermediate layer of semantic segmentation network, into a unified framework for better LLE. Such idea, i.e., the introduction of random feature, can enlighten researchers to explore more solutions for how to better leverage the latent relationships among different tasks to achieve a higher performance. In the future, we will try to adopt several model-optimization techniques, such as knowledge transfer, knowledge distillation, and model pruning, to speed up or simplify the proposed network.